CIRP Annals - Manufacturing Technology xxx (2015) xxx–xxx

Contents lists available at ScienceDirect

CIRP Annals - Manufacturing Technology

journal homepage: http://ees.elsevier.com/cirp/default.asp

Influence of SLM on shape memory and compression behaviour of NiTi scaffolds

Sasan Dadbakhsh [a,*], Mathew Speirs [a], Jean-Pierre Kruth (1)[a], Jan Van Humbeeck [b]

[a] PMA, Department of Mechanical Engineering, KU Leuven, Leuven, Belgium
[b] Department of Materials Engineering, KU Leuven, Leuven, Belgium

ARTICLE INFO

Keywords:
Selective laser melting (SLM)
Shape memory alloy
Porous structure

ABSTRACT

Octahedron-shaped porous scaffolds made from shape memory nickel–titanium (NiTi) were manufactured with different solid volume fractions using selective laser melting (SLM). Various SLM parameters were selected to affect the mechanical behaviour and shape memory response. It was shown that high laser power with high scanning speed (HP) parameters reduced the martensitic transformation temperatures as compared to low laser power low scanning speed (LP) parameters, resulting in an increased pseudoelastic behaviour (due to presence of austenite at room temperature). HP parameters, however, led to a larger geometrical mismatch with the original design and a higher solid volume fraction. The compression behaviours were also analysed and exhibited in correlation with the volume fractions.

1. Introduction

Nowadays fabrication of porous structures is receiving more attention among others to produce biomedical scaffold implants for bone replacement. Such porous materials should provide an appropriate environment for cell seeding and vascularisation and be a load bearing medium at the same time. The desired mechanical and biological properties can only be achieved from a well-controlled architecture (including volume fraction, pore size and shape, strut thickness, pore interconnectivity, etc.) in conjunction with a suitable material [1,2].

Among different possible methods to manufacture metal porous structures, selective laser melting (SLM) is specifically versatile and advantageous [3,4]. This technique is able to produce intricate porous structure architectures from metal powder materials by using a laser to melt and solidify the required geometry layer-by-layer (from a 3D CAD model) [5].

Besides the porous structure architecture, the material is of a prime importance influencing both the mechanical and biological properties. Ti alloys such as Ti–6Al–4V are the most used metal materials in SLM of porous scaffold structures [3,6], however, other promising alloys such as nickel-titanium (NiTi) are now emerging with the rapid development of SLM technology [7–9].

NiTi is a biomedical material (proven to be biologically comparable to conventional stainless steel and titanium) with a combination of high strength, ductility and low stiffness. The main application of NiTi relates to its shape recovery ability allowing implant insertion with a good mechanical stability in bone tissue applications [10]. The shape memory recovery of NiTi is due to a reversible martensitic transformation: reversible transformation of the low temperature phase (martensite with monoclinic B19′ structure) to high temperature phase (austenite with cubic B2 structure). The reversible transformation temperatures (controlling the shape memory response) are proven to be varied with processing conditions (in addition to the Ni content) [11,12]: e.g., Dadbakhsh et al. [8] have recently exhibited that different sets of SLM parameters are capable to manipulate the transformation temperatures of the bulk NiTi components. Despite this knowledge on the bulk materials, the effect of the SLM processing parameters to manufacture intricate porous structures from NiTi is still a matter of many questions. For example, it is not exactly clear how these SLM parameters influence the microstructure and also the mechanical behaviour and shape memory response of the porous structures.

This work aims at analysing the effect of SLM parameters on the shape memory response, mechanical behaviour and geometrical characteristics of porous structures. Therefore, geometrical accuracy, compression performance and transformation temperatures of NiTi porous structures (with an octahedron design and different volume fractions) will be evaluated as a function of sets of SLM parameters with contradictory influences. The main focus will be the mechanical behaviour of the scaffolds discussed based on metallurgical and geometrical differences.

2. Experimental procedure

2.1. Design and SLM

Plasma atomised NiTi powder with particle size of 25–45 μm and nominal Ni content of 55.2 wt% was provided from Raymor Industries Inc., Canada (Fig. 1). An in-house SLM machine

* Corresponding author.
E-mail address: sasan.dadbakhsh@kuleuven.be (S. Dadbakhsh).

http://dx.doi.org/10.1016/j.cirp.2015.04.039
0007-8506/© 2015 CIRP.

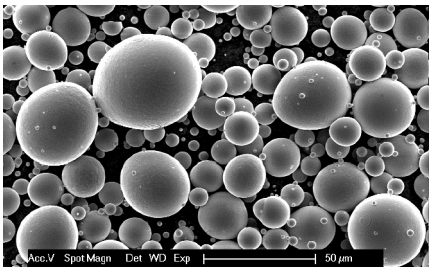

Fig. 1. SEM picture of plasma atomised NiTi powder.

Table 1
Scanning parameters used for NiTi production.

Sample	Laser power (W)	Scanning velocity (mm/s)	Hatch spacing (μm)	Energy density (J/mm^3)[a]
LP	40	160	75	111
HP	250	1100	60	126

[a] Calculated as $P/(v{\cdot}h{\cdot}t)$, where P, v, h, and t correspond to laser power, scanning speed, hatch spacing, and layer thickness, respectively.

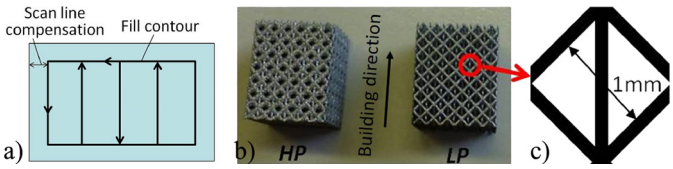

Fig. 2. (a) Hatching strategy of a strut from the top view, (b) porous scaffolds made by LP and HP parameters and (c) octahedron cell design.

(continuous 300 W Yb:YAG fibre laser with a beam diameter of about 80 μm and a galvano scanner) was used to manufacture NiTi parts under argon atmosphere with a layer thickness of 30 μm. Porous structures were manufactured in a small range of energy densities with the parameters described in Table 1 (as recommended in an earlier work [8]). High laser power adjusted to high scanning speed (HP) is to implement high heating/cooling rate in contrast to a low heating/cooling rate of low laser power low scanning speed (LP) set of parameters.

Each layer was scanned once according to the hatching strategy shown in Fig. 2a (scan line compensation of 45 μm was used). Open porous structures were designed with a simple octahedron porosity from cuboid struts of 140–300 μm and a pore size of 1000 μm (as the distance between two struts), using LP and HP parameters as shown in Fig. 2.

2.2. Materials characterisation

Micro-CT image analysis confirmed a full interconnectivity for all porous structures. Solid volume fraction of porous structures was calculated by dividing the weight of porous parts by the theoretical weight of the same bounding volume. The scaffolds were viewed using both light optical microscopy (LOM; Axiocam Leica microscope) and scanning electron microscopy (SEM; Phillips XL 30, Germany).

The transformation behaviour of porous structures was measured by DSC with a cooling/heating rate of 10 °C min^{-1} from −80 to +130 °C. Phase identification was carried out using a Siemens D500 X-ray diffractometer (XRD) with coupled Theta/2Theta scan type and Cu-Kα1 radiation operated at 40 kV and 40 mA.

To investigate the mechanical behaviour and shape memory response, the samples were compressed using an INSTRON universal testing machine with a crosshead speed of 0.2 mm/min at room temperature. The cylindrical samples were in accordance with ISO 13314 standard which requires a diameter of at least 10 times larger than the average pore size [13]. The top and bottom surfaces were lubricated using Zinc stearate beforehand.

3. Results and discussions

3.1. Geometrical characteristics

Due to the nature of continuous scanning in SLM, the galvano scanner should accelerate to reach the desired scanning speed. After finishing the defined hatching, the scanning should be de-accelerated to stop at the defined border. Although the required time/space for these accelerations and de-accelerations are very small, such small distances are very noticeable in the case of tiny struts. This imposes non-optimal lower scanning speeds, especially for the thinner struts, which in turn enlarge the melting zone. The result is a larger mismatch between the designed and produced struts (see the higher fraction difference of thinner structures in comparison with the thicker struts at Table 2).

In addition to the size of struts, the SLM parameters influence the practical mismatch of the tiny porous structures. For example, Fig. 3 evidently exhibits a higher solid fraction and thicker struts (especially along the building direction – side view) for the HP parameters compared to the LP parts (Fig. 3). This is again attributed to the required time/space for acceleration/de-acceleration. In fact, the laser needs to scan about 827 μm to reach the velocity of 1100 mm/s (as set for HP parameters), while only 115 μm is needed to reach 160 mm/s (set for LP parameters) [14]. Therefore, the energy input used for HP parameters will be much larger than the desired laser energies (lower actual scanning speed increases the energy input). This leads to a deeper laser melt pool and consequently thickened struts with high fractions (particularly along building direction) of HP parts (Fig. 3). In contrast, the LP parameters lead to more comparable fractions especially when the struts are over 250 μm thick (see Table 2).

Table 2
Solid volume fraction of scaffolds made by various parameters.

Designed strut thickness	140 μm	180 μm	250 μm	300 μm
Designed fraction	0.09	0.12	0.21	0.27
LP fraction	–	0.22	0.26	0.32
HP fraction	0.32	0.39	0.44	–

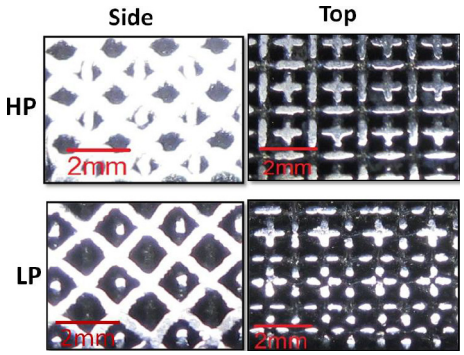

Fig. 3. Side and top views of the scaffolds made by HP and LP parameters. The struts were originally designed with 180 μm size.

3.2. Phase identification

Fig. 4 exhibits the transformation temperatures of the NiTi scaffolds, showing the microstructural features at different temperatures (varied with the SLM parameters). As seen, the HP parameters (high power + high scanning speed) lead to lower transformation temperatures compared to the LP samples. This means that the transformation of austenite to martensite during cooling (after laser melting of HP scaffolds) will occur at lower temperatures. The lower transformation temperatures of HP samples can be attributed to the associated higher heating rate followed by higher scanning speed. This promotes cooling rate, restricting precipitation and grain size, which may further stabilise the austenite subgrains [8].

Please cite this article in press as: Dadbakhsh S, et al. Influence of SLM on shape memory and compression behaviour of NiTi scaffolds. CIRP Annals - Manufacturing Technology (2015), http://dx.doi.org/10.1016/j.cirp.2015.04.039

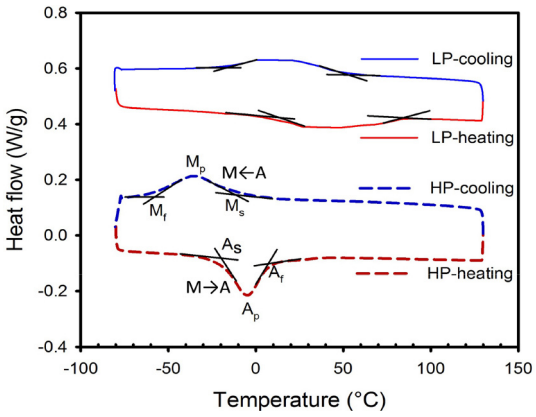

Fig. 4. DSC curves of scaffolds made by HP and LP parameters revealing the temperatures of martensitic transformations. M_s, M_p and M_f demonstrate the starting, peak, and finishing transformations of martensite upon cooling down (from austenite). Likewise, A_s, A_p and A_f are respectively starting, peak, and finishing austenite transformation temperatures during heating cycle (from martensite).

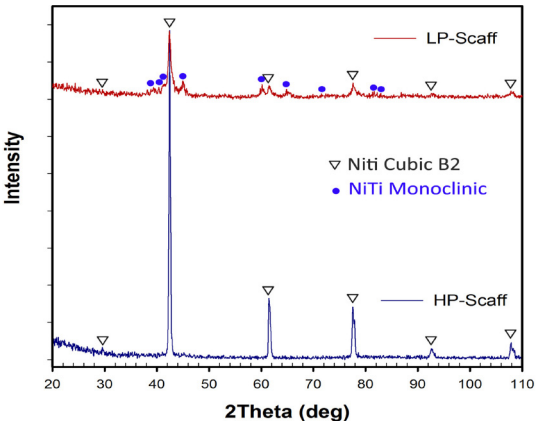

Fig. 5. XRD spectra of the SLM made NiTi scaffolds.

The effect of heating/cooling associated to the set of parameters is confirmed by the constituents at room temperature (Fig. 5); XRD detects only cubic B2 structure (demonstrating austenite) in HP scaffolds in comparison with the LP samples containing both austenite (cubic B2) and martensite (monoclinic) phases. The fully austenitic structure of HP scaffolds also implies that the formation of stress-induced martensite (originating from SLM thermal stresses) was negligible, due to the minute scanning cross sections of the scaffolds. This can be an advantage for SLM of scaffolds over the bulk NiTi components.

Accordingly, either the thermal memory (correlated to martensitic microstructure) or pseudoelasticity (from austenite) can be engineered to the scaffolds using the LP or HP parameters. This can be selected according to the desired application.

3.3. Compression behaviour

Fig. 6 shows the compressive behaviour of the NiTi scaffolds according to the SLM parameters used for their fabrication. As seen, the HP samples require a significantly higher load (e.g., few times more) in order to develop fracture compared to the LP samples. This is primarily associated with the larger volume fractions of the HP made scaffolds (imposed by the longer distance to reach the higher scanning speed). Even at comparable actual fractions (e.g., HP-s140-VF32% in Fig. 6a and LP-s300-VF32% in Fig. 6b), the HP sample is stronger mainly due to the higher solid fraction in direction of loading (HP scaffolds in side view is about twice the top view – Fig. 3) suppressing the bending of struts. Besides geometry, the higher cooling rate of HP parameters might also have led to a finer microstructure and a higher overall strength.

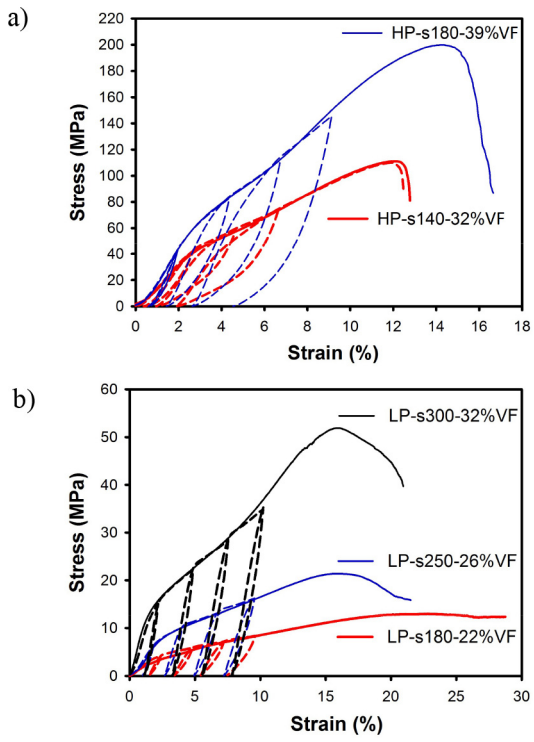

Fig. 6. Compressive stress–strain curves of the scaffolds made by (a) HP and (b) LP sets of parameters with different designed strut sizes (e.g., 180 μm) and actual solid volume fractions (%VF). Notice the scale difference.

Apart from the ultimate strength of the scaffolds (mainly varied according to the geometrical characteristics), the metallurgical properties influence the mechanical behaviour. For example, it is evident that lower transformation temperatures and austenitic structure of the HP scaffolds (Figs. 4 and 5) have led to a larger hysteresis in the compression curves (Fig. 6a). This means that HP parameters lead to a pronounced pseudoelasticity in comparison to the LP made scaffolds (due to their lower transformation temperatures). This can be used to engineer the shape memory properties of the SLM made NiTi porous structures.

3.4. Fracture/rupture analysis

The geometrical characteristics of the scaffolds, altered by SLM manufacturing parameters, affect the compression behaviour of the products. This is directly linked to the fracture mode of the scaffolds. For example, the HP made scaffolds suddenly fail with a 45° shear under compression. This is different compared to the gradual failure of LP scaffolds in which struts get separated from the nodal zones one after another (Fig. 7).

The sudden rupture of the HP scaffolds can be attributed to deformation distribution (as compressive and bending strains)

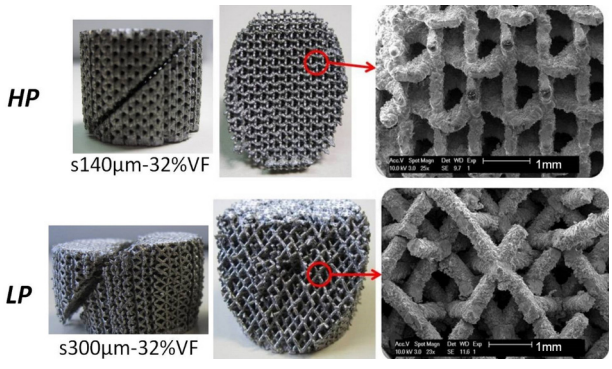

Fig. 7. Broken struts within the parts made by LP and HP parameters after compression test. The HP part is ruptured at once, while in LP, individual struts separate from the joining points during deformation. The shown strut thickness is for the CAD design not the actual product.

Please cite this article in press as: Dadbakhsh S, et al. Influence of SLM on shape memory and compression behaviour of NiTi scaffolds. CIRP Annals - Manufacturing Technology (2015), http://dx.doi.org/10.1016/j.cirp.2015.04.039

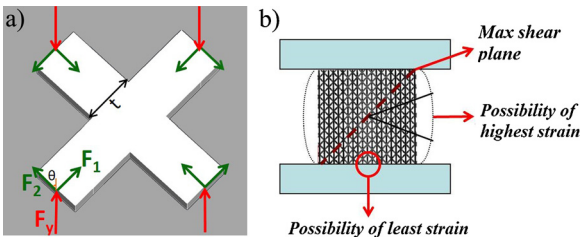

Fig. 8. Schematics of (a) struts subjected to compression and bending as a result of an applied load and (b) compression of a scaffold with the possibility of barrelling and strain localisation.

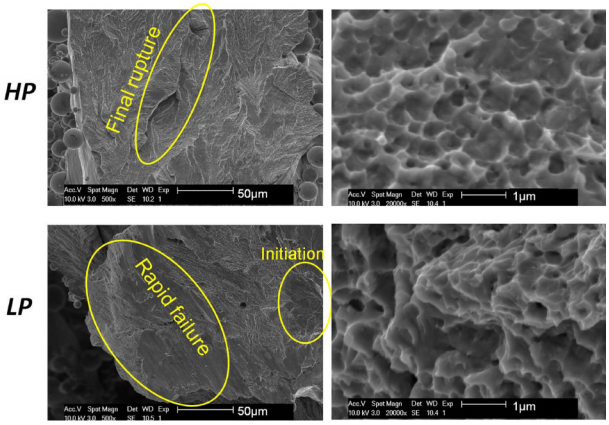

Fig. 9. Fracture surface of the struts made by LP and HP parameters.

during compression (Fig. 8). In fact, the thickened struts in HP samples first increase the bending resistance of struts; for instance the maximum bending resistance for a one-end fixed cuboid strut can be estimated as $\sigma = 6Fl/bt^2 = 6Fl/At$ where σ is stress, F is the axial load, l is the length, b is the width, A is the cross-section, and t is the thickness of the material. This means that the thicker struts (e.g., the HP struts are 2–3 times thicker than the LP ones) directly multiply the required bending loads even when the magnitude of cross-section is the same. This minimises the bending deformation and on the other hand maximises the compressive deformation (lower bending deflection promotes the axial compression ($F_1 = F_y \cdot \sin\theta$) deformation – Fig. 8a). This results in a more homogenous deformation minimising barrelling, random distortions and localised nodal failures. This postpones the final failure until all struts are loaded to their maximum shear stress. Then, upon failure the cracks develop along either of two max shear planes, i.e., 45° to the max and min stress. In contrast, the comparable width/thickness of struts made by LP parameters increases the bending deformations developing distortions in all directions. This complicates the deformation leading to local strain localisation (Fig. 8b). This results in failure of individual struts one after another and an immature drop of strength. This contributes to the lower resistance of thinner struts against bending forces leading to lower strength of LP porous scaffolds at similar volume fractions compared to the HP parts (compare Fig. 6b to Fig. 6a).

As seen from the fracture surfaces in Fig. 9, the final stage of failure in a HP strut is much smaller than a LP made strut. In other words, due to homogenous deformation in thicker struts, the crack growth stage in HP struts has been continued much longer after their initiation from all surfaces, in comparison with the LP strut that has suddenly failed due to an excessive local load after initial crack formation. However, fine microvoids/dimples as characteristics of a ductile fracture are clearly evident in both cases, implying a ductile material nature for both austenitic and martensitic microstructures (engineered by SLM parameters).

4. Conclusions

Octahedron-shaped porous scaffolds made from shape memory nickel titanium were manufactured with varying strut thicknesses and solid volume fractions using SLM. The ductile compression behaviours of the porous scaffolds were exhibited in correlation to the volume fractions. It was also shown that HP parameters (high laser power and high scanning speed) increased pseudoelastic behaviour (due to the presence of austenite at room temperature), in comparison to LP parameters that promote martensitic phases. HP parameters, however, led to a large geometrical mismatch with the original design due to a longer delay in reaching the optimal scanning speed. The non-optimal slower laser speed is very significant in the case of minute cross-sections of struts, expanding the melt pool and strut sizes. This results in a higher solid fractions and thickened struts (especially in the building direction).

Regardless of ductile characteristics of HP and LP struts, thickened struts provided a more uniform strain distribution under compressive load, in contrast to local struts failure of the LP scaffolds. The unintentionally achieved thickened struts also resulted in a better load bearing performance against directional loading (this concept can be utilised for design optimisations).

These findings can promote the manufacture of NiTi scaffolds in order to functionalise/improve the achieved properties. However, to improve the dimensional accuracy of the scaffolds made by maximal cooling rates and laser speeds, one may implement other scanning strategies (such as point scanning), which avoids the acceleration/de-acceleration of the scanner velocity in reaching highest scanning speeds.

Acknowledgment

Support is acknowledged from the EU 7th framework program (FP7) under Marie Curie ITN project BioTiNet (grant No. 264635).

References

[1] Speirs M, Humbeeck JV, Schrooten J, Luyten J, Kruth J-P (2013) The Effect of Pore Geometry on the Mechanical Properties of Selective Laser Melted Ti–13Nb–13Zr Scaffolds. *Procedia CIRP* 5:79–82.
[2] Van Bael S, Chai YC, Truscello S, Moesen M, Kerckhofs G, Van Oosterwyck H, Kruth J-P, Schrooten J (2012) The Effect of Pore Geometry on the In Vitro Biological Behavior of Human Periosteum-Derived Cells Seeded on Selective Laser-Melted Ti6Al4V Bone Scaffolds. *Acta Biomaterialia* 8:2824–2834.
[3] Van Bael S, Kerckhofs G, Moesen M, Pyka G, Schrooten J, Kruth J-P (2011) Micro-CT-Based Improvement of Geometrical and Mechanical Controllability of Selective Laser Melted Ti6Al4V Porous Structures. *Materials Science and Engineering: A* 528:7423–7431.
[4] Bartolo P, Kruth J-P, Silva J, Levy G, Malshe A, Rajurkar K, Mitsuishi M, Ciurana J, Leu M (2012) Biomedical Production of Implants by Additive Electro-Chemical and Physical Processes. *CIRP Annals* 61:635–655.
[5] Kruth J-P, Levy G, Klocke F, Childs THC (2007) Consolidation Phenomena in Laser and Powder-Bed Based Layered Manufacturing. *CIRP Annals* 56:730–759.
[6] Sallica-Leva E, Jardini AL, Fogagnolo JB (2013) Microstructure and Mechanical Behavior of Porous Ti–6Al–4V Parts Obtained by Selective Laser Melting. *Journal of the Mechanical Behavior of Biomedical Materials* 26:98–108.
[7] Bormann T, Schumacher R, Müller B, Mertmann M, de Wild M (2012) Tailoring Selective Laser Melting Process Parameters for NiTi Implants. *Journal of Materials Engineering and Performance* 21:2519–2524.
[8] Dadbakhsh S, Speirs M, Kruth J-P, Schrooten J, Luyten J, Van Humbeeck J (2014) Effect of SLM Parameters on Transformation Temperatures of Shape Memory Nickel Titanium Parts. *Advanced Engineering Materials* 16:1140–1146.
[9] Habijan T, Haberland C, Meier H, Frenzel J, Wittsiepe J, Wuwer C, Greulich C, Schildhauer TA, Köller M (2013) The Biocompatibility of Dense and Porous Nickel–Titanium Produced by Selective Laser Melting. *Materials Science and Engineering: C* 33:419–426.
[10] Bansiddhi A, Sargeant TD, Stupp SI, Dunand DC (2008) Porous NiTi for Bone Implants: A Review. *Acta Biomaterialia* 4:773–782.
[11] Zhang Y-q, Jiang S-y, Zhao Y-n, Tang M (2012) Influence of Cooling Rate on Phase Transformation and Microstructure of Ti–50.9%Ni Shape Memory Alloy. *Transactions of Nonferrous Metals Society of China* 22:2685–2690.
[12] Frenzel J, George EP, Dlouhy A, Somsen C, Wagner MFX, Eggeler G (2010) Influence of Ni on Martensitic Phase Transformations in NiTi Shape Memory Alloys. *Acta Materialia* 58:3444–3458.
[13] International Organization for Standardization (2011) *ISO 13314:2011: Mechanical Testing of Metals – Ductility Testing – Compression Test for Porous and Cellular Metals*, ISO, Genéve.
[14] Speirs M, Dadbakhsh S, Buls S, Kruth J-P, Van Humbeeck J, Schrooten J, Luyten J (2013) The Effect of SLM Parameters on Geometrical Characteristics of Open Porous NiTi Scaffolds. *6th International Conference on Advanced Research and Rapid Prototyping, VRAP*, 309–314.

Please cite this article in press as: Dadbakhsh S, et al. Influence of SLM on shape memory and compression behaviour of NiTi scaffolds. CIRP Annals - Manufacturing Technology (2015), http://dx.doi.org/10.1016/j.cirp.2015.04.039